**Proceedings of ASME Turbo Expo 2011**
**GT2011**
**June 6-10, 2011, Vancouver, British Columbia, Canada**

# GT2011-46360

# Numerical Investigation of Aerodynamic Radial and Axial Impeller Forces in a Turbocharger

**Henning Raetz, Jasper Kammeyer, Christoph K. Natkaniec, Joerg R. Seume**
Institute of Turbomachinery and Fluid Dynamics
Leibniz Universität Hannover
Appelstrasse 9
DE-30167 Hannover, Germany
E-mail: raetz@tfd.uni-hannover.de

## ABSTRACT

*Aerodynamic forces are a major cause of turbocharger bearing friction. Thus, numerical simulations with ANSYS CFX are performed for a turbocharger turbine and compressor in order to determine these forces.*
*Today, in common turbocharger CFD simulations the influence of the impeller backside cavity and blow-by are usually neglected. As a consequence, the axial forces on the impeller cannot be correctly determined. In this study therefore, the impeller backside cavity and blow-by were taken into account.*
*Additionally, the influence of different operating conditions as well as different turbine and compressor blow-by flows were investigated. Finally, the resulting aerodynamic impeller forces of a turbocharger were analysed and visualized.*
*The results show some trends which agree with the impeller forces of larger radial turbines and compressors published in literature. However some turbocharger-specific differences are identified, e.g. the wide operation range of a turbocharger. The influences of blow-by are found to be small but not negligible.*

## NOMENCLATURE

| | | |
|---|---|---|
| IBC | Impeller backside cavity | |
| BB | Blow-by mass flow rate | [g/min] |
| RMS | Root mean square | |
| r | Radius | [m] |
| s | Axial clearance between disk an casing | [m] |
| z | Distance to the IBC rotating wall | [m] |
| D | Diameter | [m] |
| $\beta$ | Air angular velocity inside the cavity | [rad/s] |
| $\omega$ | Impeller angular velocity | [rad/s] |
| $v_u$ | Absolute circumferential fluid flow velocity | [m/s] |
| $v_r$ | Absolute radial fluid flow velocity | [m/s] |
| u | Rotor circumferential velocity | [m/s] |
| k | $\beta/\omega$, ratio of angular velocity | [-] |
| $p_{st}$ | Static pressure on the impeller backside | [Pa] |
| $p_{re}$ | Reference pressure | [Pa] |
| $\nu$ | Kinematic viscosity | [m$^2$/s] |
| $y^+$ | Non-dimensional wall distance | [-] |

### Subscripts

| | |
|---|---|
| C | Compressor |
| T | Turbine |
| TC | Turbocharger |

## INTRODUCTION

Nowadays downsizing in combination with turbocharging is the most promising technology to satisfy emissions legislation. Downsizing causes undesirable transient response drawbacks of the engine. Small sized rotors with low momentums of inertia are a way to reduce the turbo lag of downsized engines. Hence the influence of turbocharger bearing friction on turbocharger dynamic performance become a new point of interest, because it directly affects the engine dynamic response. The accurate simulation of turbocharger and engine dynamic response therefore requires detailed models of the turbocharger bearings. Important boundary conditions for the development of these models are the axial and radial bearing loads. Due to the small sizes and the harsh environment of a turbocharger under real operating conditions it is difficult to measure these forces directly [1]. Furthermore most bearing systems for turbochargers inhibit a direct measurement.

For this reason different one dimensional models to predict turbocharger axial thrust are presented in literature. For example Zang presented a calculation method to predict the axial thrust of commercial turbochargers [1]. Also different studies were performed to calculate the axial thrust of turbocharges by CFD. Hanchi and Chahone [2] as well as Zhen-Xue [3] calculated the axial thrust by CFD, including blow-by.

Sun conducted numerical simulations of a 4 kg/s centrifugal compressor [4]. He stated that the impeller backside cavity flow greatly affects the axial thrust. In the literature simplified theoretical models for the impeller backside cavity flow field structure were published [5]. Usually the area between impeller and housing backplate is regarded to be parallel, vertical to the rotation axis and cylindrical. Fig. 1 represents the simplified backside cavity of these models schematically. As shown, the impeller is represented as a rotating disk with an angular speed [5].

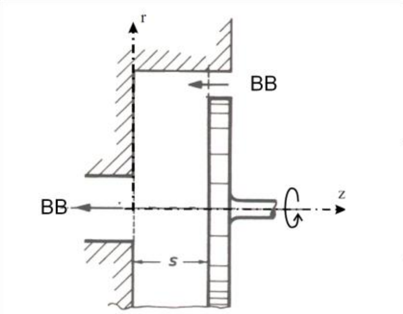


Figure 1. Model of the flow in the impeller side chamber Schilling [5].

Daily and Nece [6,7] stated four different flow regimes between a rotating smooth plane disk enclosed within a right-cylindrical chamber. Gülich studied the disk friction losses of closed turbomachinery impellers [8]. As far as the present authors know, no detailed studies were published that investigated the aerodynamic radial and axial impeller forces, accounting for the impeller backside cavity flow structure and the influences of blow-by.

Hence, this Paper presents a detailed three dimensional numerical analysis of the axial and radial aerodynamic impeller forces of a turbocharger. The main focus is on the impeller backside cavity flow structures and the influences of blow-by.

## NUMERICAL MODEL

The steady state numerical simulations were carried out with the commercial software Ansys CFX 12.1. A full-stage numerical model was created for the compressor and the turbine consisting of the domains inlet duct, volute, rotor and outlet duct. Total pressure and total temperature were set as inlet boundary condition and static pressure was set as outlet boundary condition for both, turbine and compressor. The SST turbulence model was adopted, as developed by Menter [9]. Bardina et al. [10] compared the SST model with standard k-ε and k-ω models and found it to be superior in prediction of complex flows involving separation. A frozen rotor interface was used to connect the stationary and the rotating domains of the full-stage models. Fig. 2 shows the numerical models.

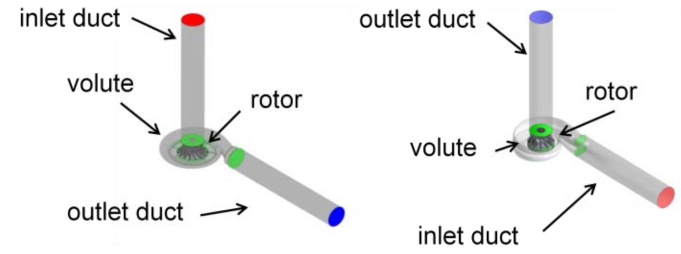


Figure 2. Numerical models.
Left: Compressor
Right: Turbine

The computational grid of the impeller is shown in Fig. 3. The impeller including the IBC is discretized with a multi-block, structured mesh. The volute is discretized by an unstructured grid.

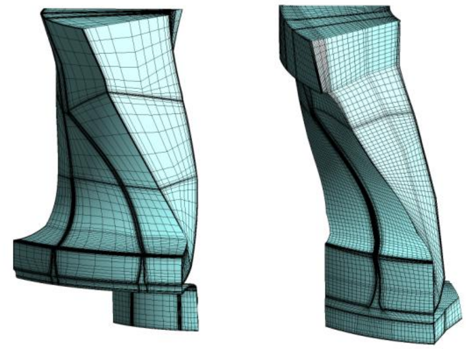

Figure 3. COMPUTATIONAL GRID OF THE IMPELLER
Left: Compressor
Right: Turbine

## ACCURACY OF NUMERICAL RESULTS

Three meshes with 2, 7 and 16 million nodes were used to verify that the numerical results are grid independent. The pressure ratio, the mass flow rate and the axial thrust were chosen as indicators for the grid convergence. A grid size of approximately 7 million nodes is found to be sufficient for the results to be independent of the grid. The $y^+$ numbers for the compressor and the turbine grids are less than 4. RMS averaged residuals, less than $10^{-4}$, were used as convergence criteria. Table 1 shows the according mesh statistics.

Table 1. Mesh statistics

| | Turbine | Compressor |
|---|---|---|
| total number of nodes | 7,201,529 | 7,214,982 |
| number of nodes in the inlet duct | 398,201 | 541,536 |
| number of nodes in the volute | 721,875 | 130,860 |
| number of nodes in the rotor | 3,724,561 | 3,689,144 |
| number of nodes in the IBC | 1,861,000 | 1,257,000 |
| number of nodes in the outlet duct | 495,110 | 426,640 |
| inlet - averaged $y+$ | 2 | 1,1 |
| volute - averaged $y+$ | 3.7 | 4 |
| rotor - averaged $y+$ | 1.8 | 2.5 |
| outlet - averaged $y+$ | 1.2 | 1.8 |

Since experimental data for the aerodynamic parameters of the IBC are not yet available, the accuracy of the numerical results has been validated against experimental data. Fig. 4 and Fig. 5 shows the numerical results compared to experimental data for the turbine and the compressor. In the following figures the mass flow rates, the pressure ratios and the efficiencies are normalized with the global maximum values for the turbine or the compressor.

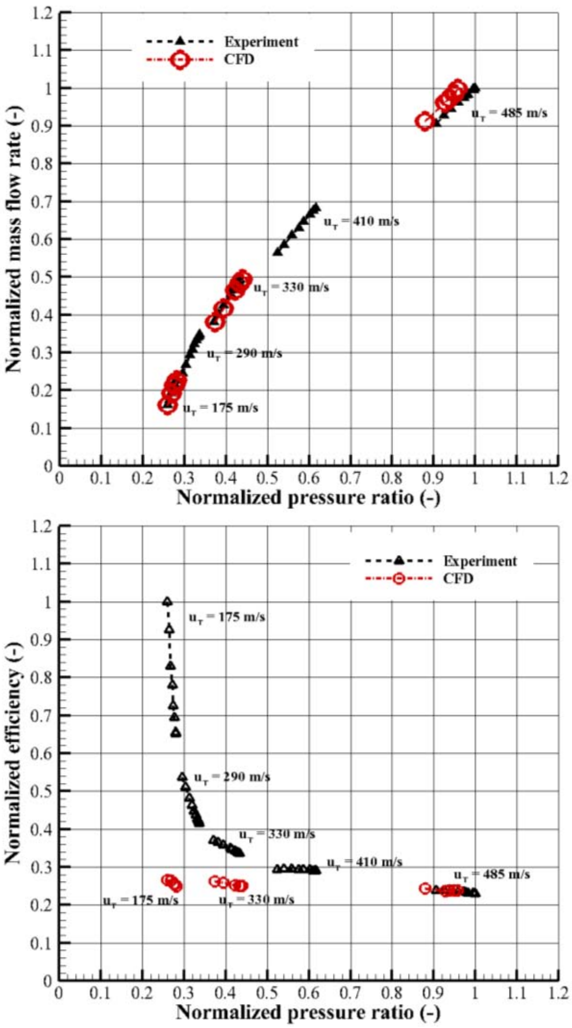


Figure 4. Comparison of the numerical results to experimental data for the turbine.

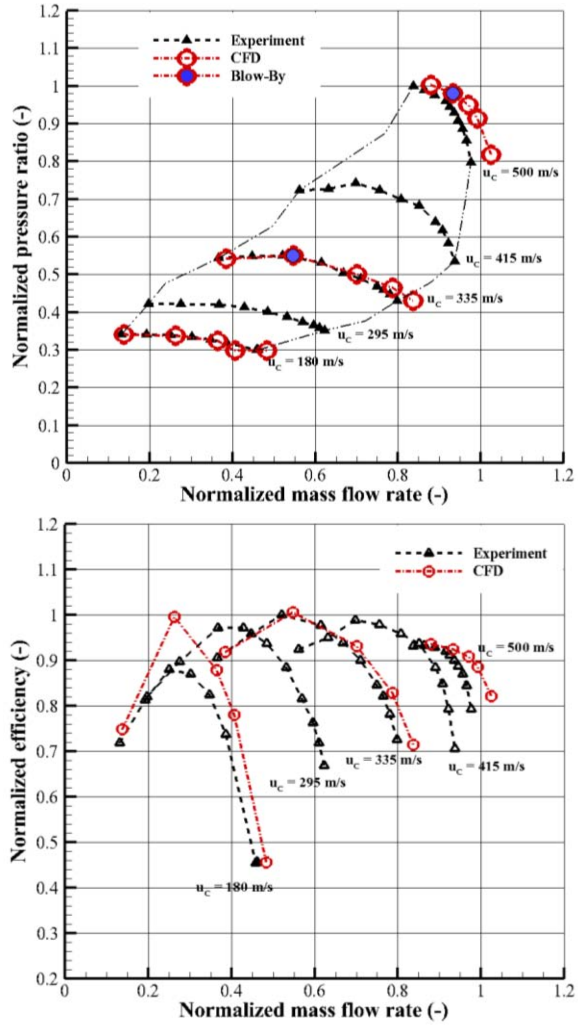


Figure 5. Comparison of the numerical results to experimental data for the compressor.

The numerical results are in good agreement with the experimental data. The deviation of the mass flow for the compressor and the pressure ratio for the turbine are at maximum 5 percent. The pressure ratio characteristic for constant speed lines shows a good agreement. The deviation of the efficiency is caused by non adiabatic effects, causing an underestimation of the measured diabatic compressor efficiency and a overestimation of the turbine efficiency on a turbocharger test stand [11].

## PROCEDURE

Fifteen operating points (marked red in the compressor map) were selected for the steady state numerical analysis of the turbine and the compressor covering a wide operating range (c.f. Fig. 5). The influences of blow-by were investigated for two significant operating points (marked blue in the compressor map) at design and maximum speed. At these operating points blow-by flow rates of BB=0 g/min, BB=12 g/min and BB=50 g/min were set at the compressor and turbine side. BB=50 g/min is 0.23 percent of the maximum global compressor mass flow rate and 0.2 percent of the maximum global turbine mass flow rate.

## AXIAL IMPELLER FORCES

The unbalance of the axial rotor forces on the compressor and the turbine side results in the axial thrust of the turbocharger. The rotor forces appear due to static pressure distributions on all surfaces of the wheels and flow momentum forces. In a normal back-to-back arrangement the net forces acting on the compressor and the turbine will tend to cancel each other [12]. In this study the axial thrust of the impeller is calculated by integrating the static pressure fields on the front- and the backsides of the wheels.

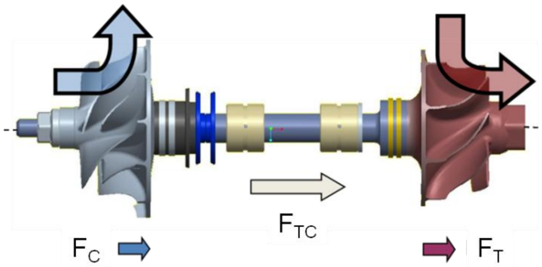


Figure 6. Scheme of axial thrusts for a turbocharger.

In the following the calculated axial forces of the numerical analyses in the direction defined in Fig. 6 are presented. Figure 7 displays the axial impeller forces on the turbine side. As expected, the forces increase with mass flow and inlet pressure of the turbine.

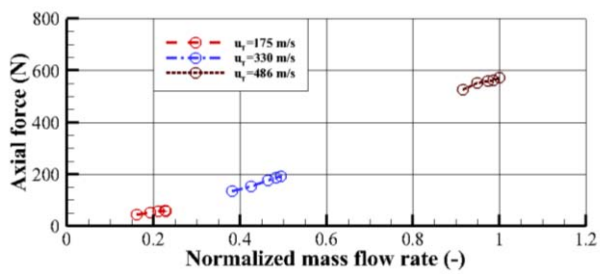


Figure 7. Axial impeller forces on the turbine side.

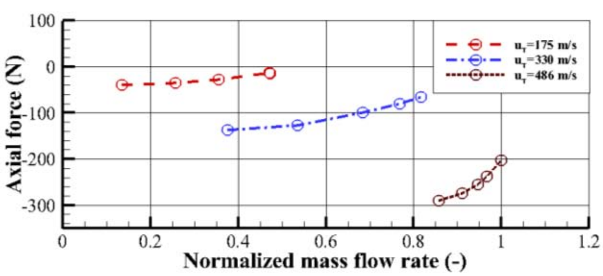


Figure 8. Axial impeller forces on the compressor side.

The axial impeller forces of the compressor side are shown in Fig. 8. In this case the forces on the frontside and the backside of the impeller are dominated by the compressor outlet pressure. Again the momentum force depends on the mass flow rate. The absolute maximum of the overall axial force is located at the surge line and the minimum is found at the choke line, while the devolutions show the same characteristic as the related compressor performance lines.

Fig. 9 displays the resulting axial thrusts of the investigated turbocharger over the normalized compressor mass flow rate. Due to the same impeller diameter of the turbocharger used in this study the axial thrust has no zero-crossing. The axial thrust is approximately in balance at design point but increases at off design conditions. A continuous increase of axial thrust was found from surge to choke and with mass flow.

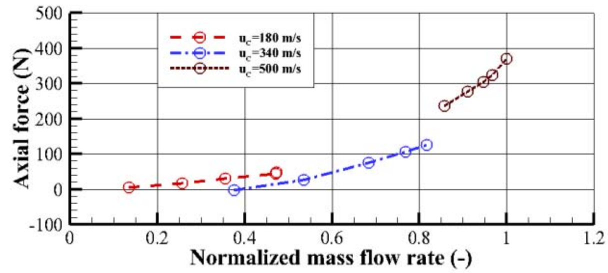


Figure 9. Resulting axial thrust of the turbocharger.

The relationship between the pressure ratio of the compressor and the turbine is a function of the efficiencies of the turbocharger, as well as the temperatures at the inlet of the compressor and the turbine [12]. The requirement for a higher compressor pressure ratio is higher total turbocharger efficiency and a higher temperature at turbine inlet. The decreasing pressure ratio and efficiency of the compressor near choke and at off design points lead to a higher turbine pressure ratio. Thus, the turbine seems to dominate the characteristic of the axial thrust.

## RADIAL IMPELLER FORCES

During off design conditions centrifugal impellers possess non axis-symmetric circumferential pressure distributions due to non uniform flow in the volutes [13,14]. This non uniform pressure distributions cause a circumferential variation of the impeller blade loading. As a consequence an aerodynamic radial impeller force appears with a maximum at choke line, followed by a minimum at maximum efficiency and a moderate increase in the direction of the surge line [15].

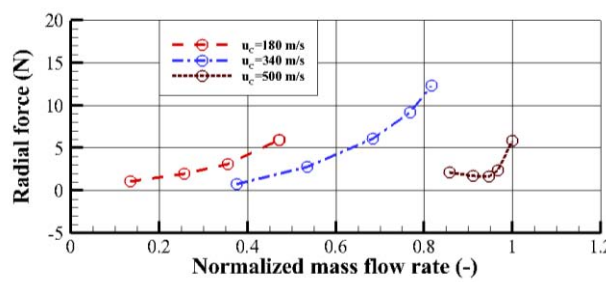


Figure 10. Radial impeller forces on the compressor side.

The calculated radial impeller forces are shown in Fig. 10 for the compressor side. Only for the maximum speed line the characteristic described by Reunanen [15] was found. The other two speed lines only show the right part of the devolution. The non-uniformity pressure distributions, causing the radial force, are driven by the compressor efficiency and negative effects related to it are strong especially at high mass flow rates and off design conditions.

The calculated radial impeller forces for the turbine side are shown in Fig. 11. Due to the small operating range of a turbocharger turbine operating on a turbocharger test stand the pressure distributions in the volute, causing the radial force, is small [10]. Almost no aerodynamic radial impeller forces were found for the lower two speed lines. For the high speed line values of about 5 N were calculated, while no obvious characteristic was found over the speed line.

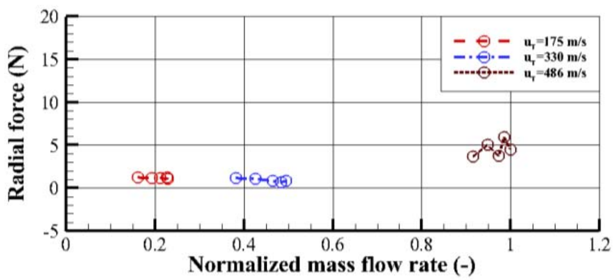


Figure 11. Radial impeller forces on the turbine side.

## IBC STRUCTURES

An important dimensionless parameters for the modeling of the impeller backside cavity is the Reynolds number

$$Re = \frac{\omega \cdot r^2}{\nu} \qquad (1)$$

of the flow in the backside cavity. In Eq. (1) the radius $r$ of the impeller backside is chosen as specific length. Zilling [16] conducted investigations of the flow field in the backside cavities of radial pumps. He presented four different regimes of flow conditions that appear depending on the boundary conditions, e.g impeller speed and gap width. Table 2 gives an overview of these flow regimes.

Table 2. Flow regimes in the impeller backside cavity for different Reynolds numbers [15]

| Regime | Condition | Boundary layer | Range |
|---|---|---|---|
| 1 | Laminar flow | Merged boundary layers | $Re<1*10^3$ |
| 2 | Laminar flow | Separated boundary layers | $Re<1*10^5$ |
| 3 | Turbulent flow | Merged boundary layers | $1*10^5<Re<5*10^5$ |
| 4 | Turbulent flow | Separated boundary layers | $Re>5*10^5$ |

An overview of different studies of the flow field in the backside cavities of radial impellers can be found at Schilling [5]. Also the global Reynolds number (Eq. 1) is used to classify the flow characteristics. Fig. 12 shows the investigated flow fields of Schilling [5].

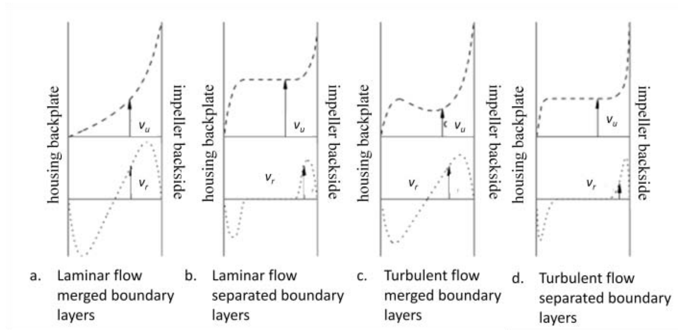


Figure 12. Flow fields in the impeller backside cavities for different flow regimes [5].

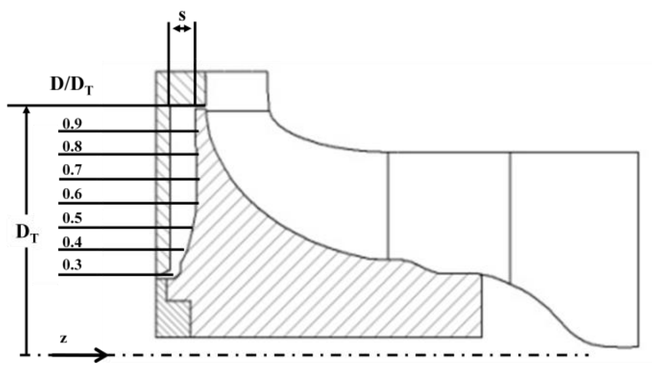


Figure 13. Intersection of the turbine impeller backside cavities with the seven implemented planes.

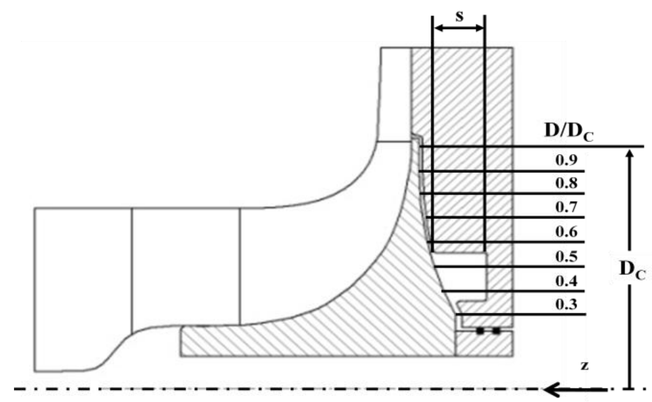


Figure14. Intersection of the compressor impeller backside cavities with the seven implemented cylindrical surfaces.

The IBC geometry is axisymmetric, so the aerodynamic parameters of the IBC are almost constant in the circumferential direction except for the regions near the gap between the backplate tip and the housing, where the IBC aerodynamic parameter distributions are greatly affected by the uneven static pressure distribution at the impeller exit [1]. As stated, the appearing flow characteristics in the impeller backside cavity are also related to the gap width s. In tight impeller backside cavities, the boundary layers are expected to touch each other, while the boundary layers in wider impeller backside cavities are separated. In case of separated boundary layers, a core flow of constant circumferential velocity appears in the gap (c.f. Fig. 12 and Table 2).

In the present study, seven cylindrical surfaces were implemented at different diameter ratios to analyze the flow field structure in the impeller backside cavities, as shown in Fig. 13 for the turbine side and Fig. 14 for the compressor side. Fig. 15 to Fig. 17 display the calculated circumferential averaged velocity profiles of the circumferential velocity and the radial velocity in the turbine backside cavity, normalized with the circumferential impeller velocity. The results are presented for seven different diameter ratios according to the cylindrical surfaces in Fig. 13 on the turbine side. The abscissa represents the z-direction which is normalized with the gap width s. For the turbine side Reynolds numbers of Re = $0.75*10^5$, $1.25*10^5$ and $2*10^5$ were considered.

The velocities in circumferential and radial direction add up to a complex vortex structure which is shown in Fig. 18 for the intersection of the turbine backside cavity. Transport processes by friction and diffusion are physically predominant for creeping flow between a rotating impeller and a fixed housing. A fluid particle adheres at the rotating impeller backside and the next fluid particle is accelerated in circumferential direction by friction between the two floating particles. The motion of particles farther away from the two walls occurs in layers. Fluid particles moving in circumferential direction are affected by centrifugal forces that accelerate the flow in radial direction. Thus a flow in radial direction is caused by the radial momentum imbalances. Once the flow reaches the fixed wall at the radial end of the cavity it is backed up and turns back inwards to decreasing diameters on the side of the housing. In the area of small disk diameters, the flow is turned back into the direction of the rotating impeller backplate which again accelerates the flow to the outside of the gap.

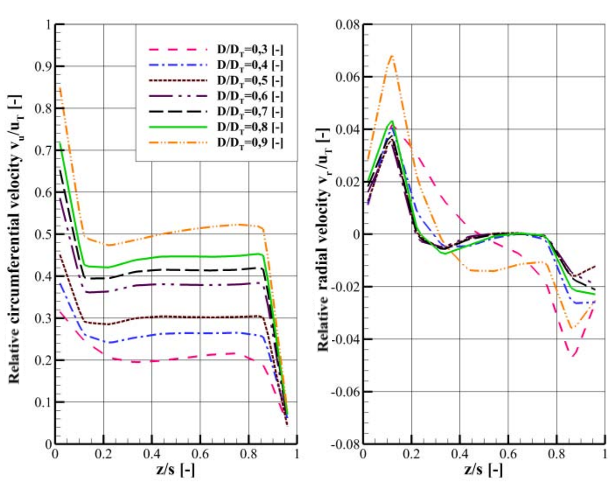


Figure 15. Calculated velocity profiles for the turbine backside cavity at Re = $0,75*10^5$.

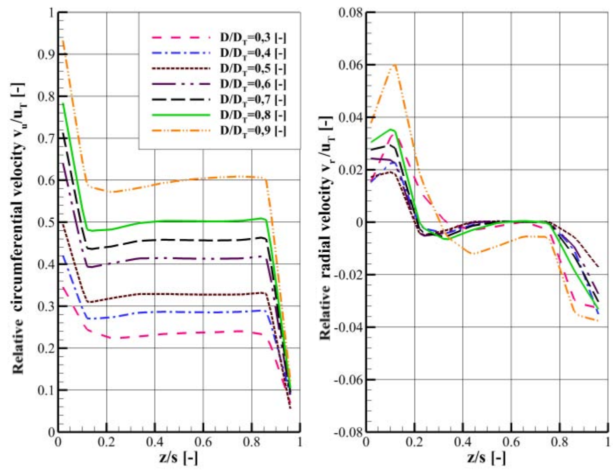


Figure 16. Calculated velocity profiles for the turbine backside cavity at Re = $1,25*10^5$.

With increasing Reynolds numbers (increasing impeller speeds), the inner friction of the fluid in the gap becomes less dominant. The flow is turbulent for Reynolds numbers higher than Re = $10^5$. Thus the velocity profiles represent laminar flow characteristics in Fig. 15 and turbulent flow characteristics in Fig 16 and Fig. 17. It is obvious, that turbulent flow conditions lead to increasing velocity gradients at the walls of the rotating impeller and the stagnating housing $|\delta v_u/\delta z|$ and $|\delta v_r/\delta z|$. Hence, the area of the core flow of constant circumferential and radial velocity (solid body vortex) increases with Reynolds number.

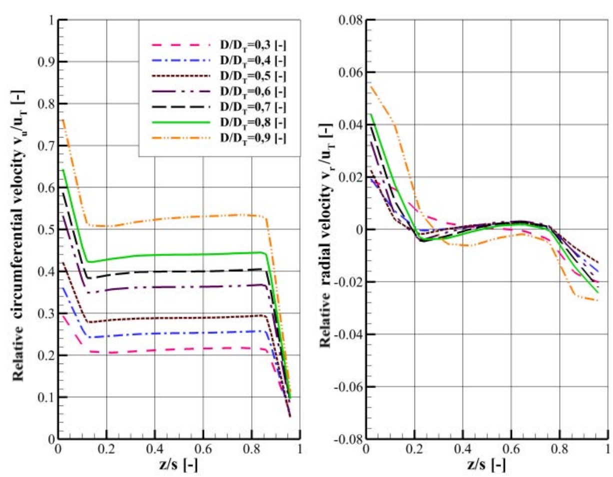


Figure 17. Calculated velocity profiles for the turbine backside cavity at Re = $2*10^5$.

The velocity profiles of the radial velocity show a local maximum, a turning point and a local minimum. The maximum and minimum of the almost sinusoidal radial velocity profile are moved closer to the walls with increasing Reynolds number, as shown in Fig. 15 to Fig. 17.

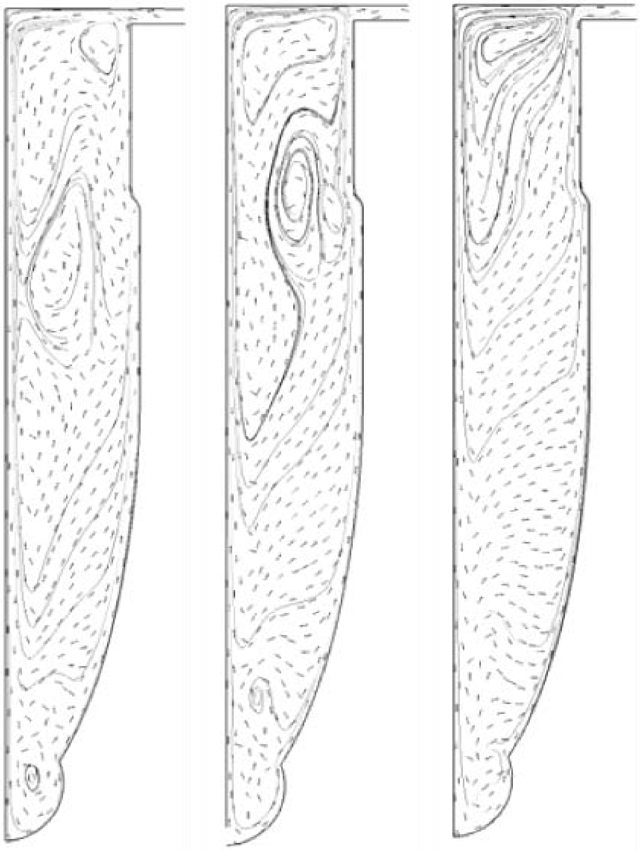

Figure 18. Vortex structures in the intersection of the turbine impeller backside cavity (without blow-by).
Left: Re = 0.75*$10^5$
Center: Re = 1.25*$10^5$
Right: Re = 2*$10^5$.

Also for increasing Reynolds numbers, the core of the radial vortex structure in the impeller backside cavity of the turbine moves to larger diameters, as shown in Fig. 18. The vortex structure is displayed by velocity vectors and streamlines projected on the meridional plane. This is caused by rising centrifugal forces affecting the fluid particles in the gap. Also the vortex core becomes smaller, because it is pushed into the outer housing corner of the cavity. The pressure fields in the turbine backside cavity according to the flow structures of Fig. 18 show small pressure gradients in radial direction for low Reynolds numbers. However, an unequal pressure distribution appears due to the large-area vortex structures. With increasing Reynolds number the pressure gradient in radial direction rises, but the pressure distribution becomes more homogeneous.

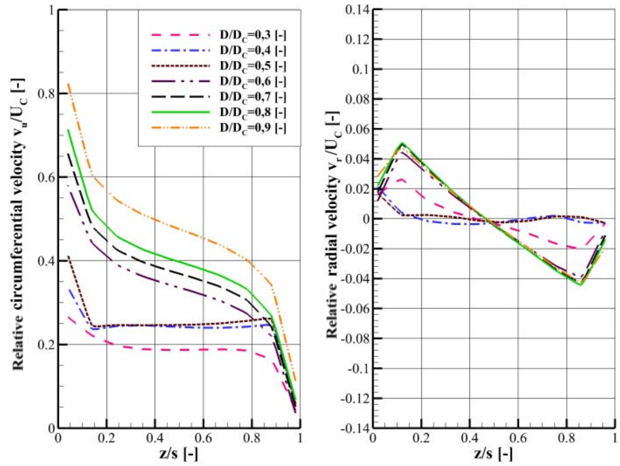


Figure 19. Calculated velocity profiles for the compressor backside cavity at Re = 2,6*$10^5$.

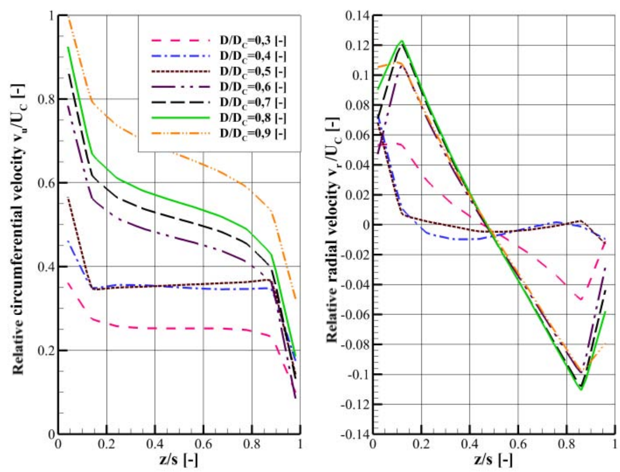


Figure 20. Calculated velocity profiles for the compressor backside cavity at Re = 7.4*$10^5$.

Fig. 19 to Fig. 20 displays the analogous velocity profiles of the compressor backside cavity. The results are also presented for same seven different diameter ratios according to the planes in Fig. 14 on the compressor side. Again the abscissa represents the z-direction which is normalized with the gap width s. For the compressor side Reynolds numbers of Re = 2.6*$10^5$ and 7.4*$10^5$ were considered.

The compressor backside cavity has a small gap for 0.55<$D/D_C$<1. At diameter ratios of $0.35 < D/D_C < 0.55$ a big broadening is located in the compressor backside cavity. This design of the backside cavity leads to some special characteristics of the velocity profiles.

In the small gap at 0.55<$D/D_C$<1 the velocity profiles of the compressor backside cavity show some deviations compared to the turbine side. In this area the velocity gradients on the walls of the rotating compressor impeller and the stagnating housing $|\delta v_u/\delta z|$ and $|\delta v_r/\delta z|$ are smaller, compared to the turbine. Hence, the area of the core flow of constant circumferential and radial velocity (solid body vortex) is also less dominant and barely existing at high diameter ratios. The radial velocity profiles in this area show a severe minimum and maximum with a linear devolution without turning point in between. Thus merged boundary layers seem to predominate the flow.

In the broadening at $0.35 < D/D_C < 0.55$ the velocity profiles are more similar to the turbine backside cavity (c.f. Fig. 15 to Fig. 17). The broadening of the compressor backside cavity also affects the flow structure behind the impeller. A complex radial vortex structure and separated boundary layers appear in this broadening of the gap section, as shown in Fig. 21 for the intersection of the compressor backside cavity. For increasing Reynolds numbers the vortex structures become more severe and a larger number of vortex cores appear.

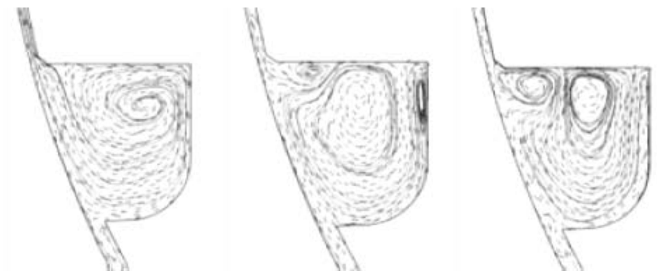

Figure21. Vortex structures in the intersection of the compressor impeller backside cavity (without blow-by).
Left: Re = 2.6*10^5
Center: Re = 5*10^5
Right: Re = 7.2*10^5.

## INFLUENCE OF BLOW-BY FLOW

In the following the influences of blow-by on the backside cavity flow structures of the two impellers are presented.

Fig. 22 and Fig. 23 show the circumferential and radial velocity profiles of the turbine backside cavity for BB = 12 and 50 g/min. The circumferential velocities were found to decrease with blow-by, especially at low diameter ratios (shaft seal area). This effect can be explained by less creeping flow that is dragged between impeller backside and housing. In contrary the radial velocities increase with blow-by, caused by secondary flows in the backside cavities.

In case of blow-by, the flow field is affected by an additional velocity component in the direction to the shaft (opposite direction of centrifugal forces). On its way through the backside cavity, the blow-by flow interacts with the main cavity vortex. As a consequence most of the blow-by is deflected in the direction of the stagnating housing wall, where it flows towards the shaft seal. Thus a stronger increase of the radial velocities can be observed at the housing wall, compared to the impeller backside (c.f. Fig. 22 and Fig. 23). However, the swirl velocity of the main radial cavity vortex also rises.

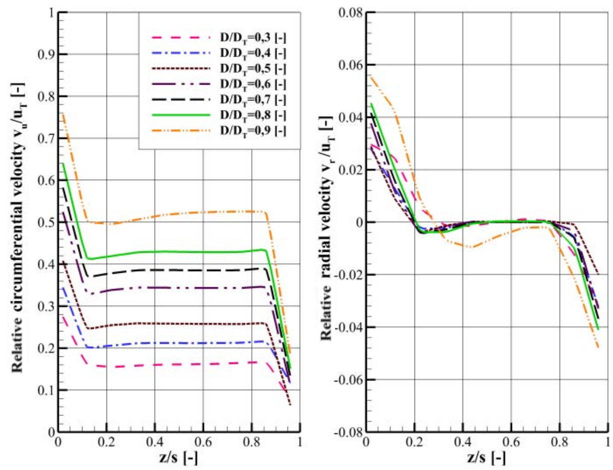


Figure 22. Calculated velocity profiles for the turbine backside cavity at Re = 2*10^5 and BB = 12 g/min.

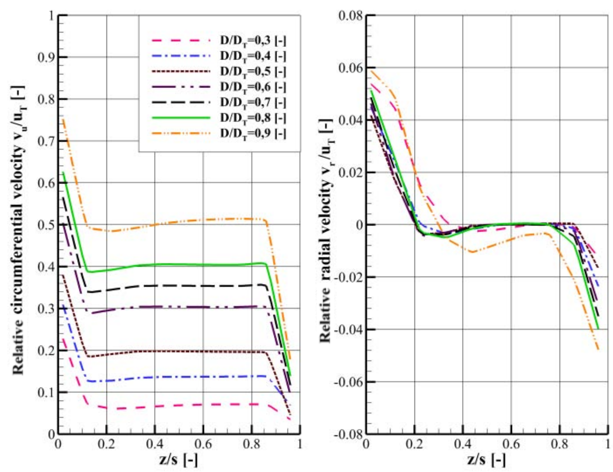


Figure 23. Calculated velocity profiles for the turbine backside cavity at Re = 2*10^5 and BB = 50 g/min.

Due to the increase of radial vortex swirl, less energy is left for the rotation of flow in circumferential direction (solid body vortex). This effect is shown in Fig. 24 and Fig. 25 for different blow-by flow rates, by the relative fluid rotation of the circumferential vortex $k = \beta/\omega$. This fluid rotation of the circumferential vortex is usually described by the ratio of fluid velocity $v_u$ to impeller circumferential velocity $u = \omega \cdot r$ and expressed by the rotation factor

$$k = \frac{v_u}{u} = \frac{v_u}{\omega \cdot r} = \frac{\beta}{\omega} \qquad (2)$$

As shown, the relative angular fluid velocity k possesses an almost constant value of k = 0.5 over the diameter ratio, for zero blow-by Thus the fluid forms a kind of solid-body rotation with a constant angular velocity $k_0$ [8].
Fig. 24 shows the calculated relative fluid rotation of the circumferential vortex for different blow-by flow rates. It is obvious, that the fluid rotation decreases with blow-by. Again the major influences were found in the shaft seal area. These

characteristics show a good correlation with results of Gantar et al. [16] (c.f. Fig. 25).

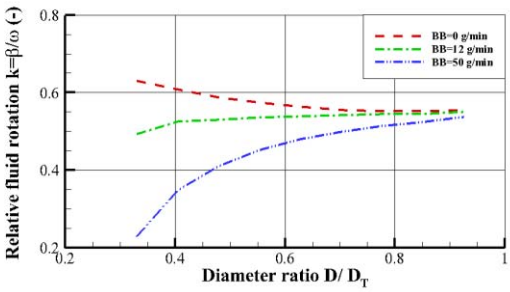


Figure 24. Relative fluid rotation of the circumferential vortex on the turbine side for BB = 0, 12 and 50 g/min.

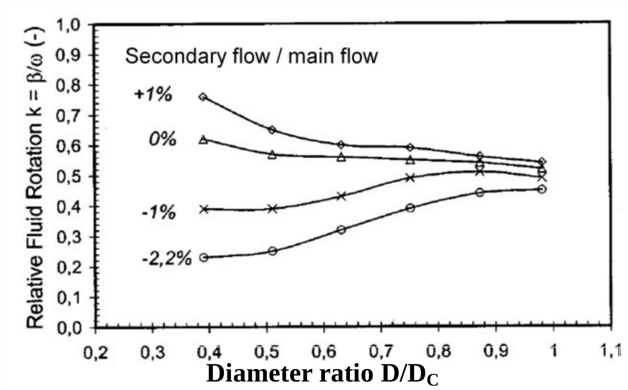


Figure 25. Relative fluid rotation in the impeller backside cavity [16]

Due to the rotation of the impellers, centrifugal forces affect the fluid particles in the backside cavities. This effect causes a static pressure gradient from shaft to outer wheel diameter. This pressure gradient changes with blow-by.

The static pressure distributions in the impeller backside cavity for different blow-by flow rates and Reynolds numbers are shown in Fig. 26, for the turbine and the compressor side.

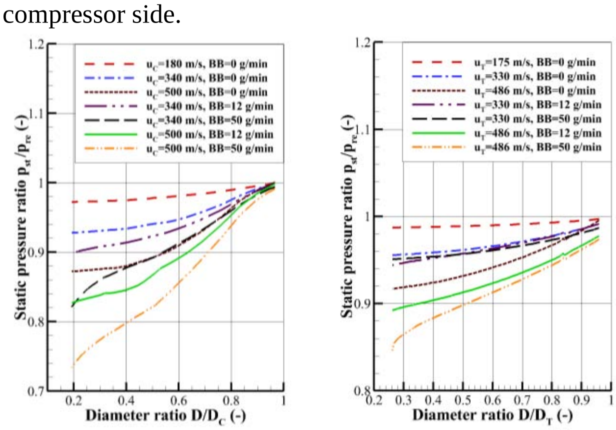


Figure 26. Static pressure distributions on the casing
Left: Compressor
Right: Turbine

The pressure is normalized with the pressure at the interface from impeller and IBC. It is obvious, that blow-by affects the pressure distribution in the backside cavities of the impellers. As expected the influences are more distinct in the area of the shaft seals, where the blow-by flow exits the backside cavity. In this area changes of the static pressure ratio of up to 14 % were calculated. This static pressure drop is mainly caused by the fact, that in case of blow-by the fluid is accelerated into the narrowing flow cross-section in the direction to the shaft seal.

The decrease of the static pressure ratios in the impeller backside cavity with increasing blow-by flow leads to decreasing axial forces for both impellers, as shown in Fig. 27 for the turbine and in Fig. 28. for the compressor. Thereby the variation of turbine axial forces is about 30 N for the investigated blow-by flow rates. The analogous variation of the compressor axial forces is about 40 N. Due to the reverse direction of the axial turbine and compressor forces, the changes of the turbocharger axial thrust due to blow-by were approximately 5 N.

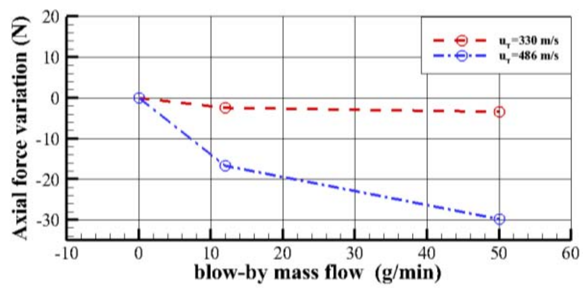


Figure 27. Turbine axial force variation due to different blow-by flow rates.

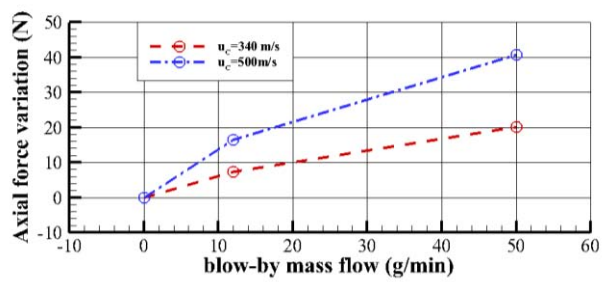


Figure 28. Compressor axial force variation due to different blow-by flow rates.

## CONCLUSIONS

In the present paper the aerodynamic rotor forces in a turbocharger were analyzed over a wide operating range, the impeller backside cavity and the blow-by leakage flow were taking into account.

The aerodynamic radial impeller forces of the compressor show some trends which agree with larger centrifugal compressors. For both, the turbine and the compressor side, the aerodynamic radial impeller forces were found to be very small compared to the axial impeller forces. The dynamic radial forces caused by the unbalance and dynamic behavior of the rotor probably are assumed a lot larger than the aerodynamic radial forces calculated in this study.

The basic flow field structure of the impeller backside cavities was found to be approximately uniform in the circumferential direction. However, in radial direction severe gradients of static pressure were found, which are mainly driven by centrifugal forces. Thus, complex pressure distributions appear in the backside cavities which strongly impact the aerodynamic axial impeller forces.

Not considering blow-by, a substantial overall maximum axial thrust of 385 N was calculated in this study. This value was found at a circumferential compressor impeller speed of 500 m/s. The aerodynamic radial impeller forces did not exceed 13 N for the whole operating range.

The blow-by flow strongly affects the axial forces on the turbine and the compressor side due to sensible influences on the flow field structures in the impeller cavities. Thus, axial force variations due to blow-by, at the design point and a blow-by mass flow of 12 g/min, of up to 1.9 percent (3 N) on the turbine side and up to 6.3 percent (8 N) on the compressor side were found. Due to the reverse direction of the axial turbine and compressor forces, the changes of the turbocharger axial thrust due to blow-by were approximately 20 percent (5 N), at a circumferential compressor impeller speed of 340 m/s.

From the experience gained in this study, it is highly recommended to account for realistic impeller backside cavity geometries, when calculating accurate aerodynamic axial impeller forces in a turbocharger by numerical simulations.

## ACKNOWLEDGMENTS

The work was supported by the Forschungsvereinigung Verbrennungskraftmaschinen e. V. (FVV) whose funding is gratefully acknowledged. Also the authors would like to thank the Voith Turbo Aufladungssysteme GmbH & Co. and the ”North-German Supercomputing Alliance” for supporting this study. In addition, the authors would also like to thank Mr. T. Kentschke and Mr. F. Wilkening for the help during the numerical studies.

## REFERENCES

[1] Zhang, D., Sun, Z., 2010, “Fault Diagnosis and Failure Prediction by Thrust Load Analysis for a Turbocharger Thrust Bearing,” ASME Paper, GT2010-22320

[2] Hong Hanchi and Ma Chaochen, 2006, “Numerical Solution of Axial Thrust of Turbochargers.”, VEHICLE AND POWER, 2006-2

[3] Zhen-Xue Han, Paul G. A., Cizmas, 2001, “A CFD Method For Axial Thrust Load Prediction of Centrifugal Compressors”, ASME Paper No. 2001-GT-0568.

[4] Sun, Z., Tan, C., Zhang, D., 2009, “Flow field structures on the impeller backside cavity and its influences on the centrifugal compressor,” ASME Paper, GT2009-59879

[5] Schilling, R.: Strömung in Radseitenräumen von Kreiselpumpen. In: Strömungsmechanik und Strömungsmaschinen 27 (1979), S. 21–86. – Habilitationsschrift; TH Karlsruhe

[6] Daily, J. W., and Nece, R. E., 1960, „Roughness Effects on Frictional Resistance of Enclosed Rotating Disks“, Trans. ASME, Journal of Basic Engineering, Vol. 82, pp. 553-562

[7] Nece, R. E., and Daily, J. W., 1960, „Chamber dimension Effects on Induced Flow and Frictional Resistance of Enclosed Rotating Disks“, Trans. ASME, Journal of Basic Engineering, Vol. 82, pp. 217-232

[8] Gulich, J. F., 2003, “Disk Friction Losses of Closed Turbomaschine Impellers”, Forschung im Ingeniuerwesen, Vol. 68, pp. 87-95

[9] Menter, F. R., 1994, “Two-equation eddy-viscosity turbulence models for engineering applications.”, AIAA Journal, Vol. 32, No. 8, pp. 1598-1605

[10] Bardina, J. E.; Huang, P. G.; Coakley, T. J.: Turbulence Modeling Validation, Testing and Development. NASA Technical Memorandum 110446, 1997

[11] Shaaban, S., Seume, J., 2006, “Analysis of turbochargers non-adiabatic performance.” Proceedings of 8th International Conference on Turbochargers and Turbocharging, London, UK, C647/027

[12] Baines N. C., 2005 “Fundamentals of Turbocharging”, Cocepts NRCE Inc., Vermont

[13] Steglich, T., Kitzinger, J., Seume, J., Van den Brembusche, R., Prinsier, J., 2008, “Improved Diffuser/Volute Combinations for Centrifugal Compressors”, Trans. ASME, Journal of Turbomachinery, Vol. 130

[14] Shaaban, S., Seume, J., 2007, “Aerodynamic performance of small turbocharger compressors.” ASME Paper No. GT-2007-27558

[15] Reunanen, A., Larjola, J., 2005, “Radial forces in a centrifugal compressor; experimental investigation by using magnetic bearings and static pressure distribution.” Journal of Thermal Science, Vol. 14, No 1, pp. 1-8

[16] Zilling, H.: „Untersuchung des Axialschubes und der Strömungsvorgänge in den Radseitenräumen einer einstufigen radialen Kreiselpumpe mit Leitrad.“ Sonderdruck Aus: Strömungsmechanik und Strömungsmaschinen 15, Universität (TH) Karlsruhe,1973

[17] Gantar, M., Florjancic, D. and Sirok, B., 2002, “Hydraulic Axial Thrust in Multistage Pumps-Origins and Solutions”, Journal of Fluids Engineering, Vol. 124, pp. 336-341